

Micromechanisms of short fatigue crack growth in an Al-Si piston alloy.

T.O. Mbuya¹, and P.A.S. Reed

Engineering Materials Group, Faculty of Engineering and the Environment, Highfield, University of Southampton, SO17 1BJ, UK.

Published in Materials Science & Engineering A (2014), pp. 302-309

DOI information: 10.1016/j.msea.2014.06.046

Authors' copy of refereed paper

Abstract

The short fatigue crack growth behaviour of a model cast aluminium piston alloy has been investigated. This has been achieved using a combination of fatigue crack replication methods at various intervals during fatigue testing and post-mortem analysis of the crack profiles. Crack-microstructure interactions have been clearly delineated using a combination of optical microscopy and scanning electron microscopy. Results show that intermetallic particles and eutectic Al-Si regions play a significant role in determining the crack path and growth rate of short fatigue cracks. It is observed that the growth of short cracks is often retarded or even arrested at intermetallic particles and Al-Si eutectic regions. Crack deflection at intermetallics and eutectic Si is also frequently observed. These results have been compared with the long crack growth behaviour of the alloy.

Keywords: Fatigue; Short fatigue cracks; Fatigue micromechanics; Al-Si ; Fatigue ; piston alloys

1. Introduction

Light vehicle engine pistons are commonly cast from near-eutectic multicomponent Al-Si alloys typically containing high levels of Cu and Ni [1]. The rapid increase in performance requirements in diesel engines together with light-weighting and strict emission regulations has necessitated development of new piston designs and materials that can withstand the increasingly harsh combination of fluctuating thermal stresses and cylinder pressure [2,3]. As a result, new alloys have been developed with increasingly higher levels of various alloying elements such as Cu to upwards of 4-5 wt.% and Ni to ~3 wt.% [3,4]. Hypereutectic silicon levels have been suggested [4], but low Si alloys have also been proposed [5] to mitigate against fatigue crack initiation at primary Si particles as often observed in the near-eutectic Al-Si piston alloys [6]. These new alloys have been shown to have complex and three-dimensionally networked microstructure [1]. The successful application of these alloys in modern pistons requires a thorough characterization of their microstructure and the micromechanics of fatigue failure.

Previous work by Joyce et al. [6] indicated that fatigue cracking in two near-eutectic Al-Si piston alloys occurred mostly at primary Si particles at both room and high temperatures (200°C and 350°C). However, limited crack initiation at clusters of $Al_3(Cu,Ni)_2$ particles was also observed, but only in the alloy with higher Cu (3.1 wt.%) and Ni (2.27 wt.%) contents.

¹Corresponding author. Current contacts and address: Tel. +254 020 318262 ext. 28383; *E-mail address* - tmbuya@uonbi.ac.ke; Department of Mechanical and Manufacturing Engineering, University of Nairobi, P.O. 30197, 00100 (GPO), Nairobi, Kenya.

In the alloy with low Cu (0.94 wt.%) and Ni (0.96 wt.%) contents, initiation was observed to occur exclusively at fractured Si particles. The authors suggested that intermetallic particles may dominate the fatigue process in the absence of primary Si particles.

Previous studies [1,3,7,8] on model piston alloys with high Cu and Ni levels (3.9 wt.% Cu and 2.8 wt.%Ni) confirmed that fatigue crack initiation occurs at Si particles and intermetallic particles such as Al_9FeNi and $Al_3(CuNi)_2$. Some of the model alloys investigated contained reduced Si levels of 6.9 wt.% and 0.67 wt.% as shown in Table 1. The authors observed crack initiation to occur mainly at intermetallic particles and porosity in the 6.9 wt.% Si alloy but exclusively at pores in the low Si (0.67 wt.%) alloy. Moreover, although short fatigue cracks were observed to interact strongly with intermetallic particles in all alloys investigated, the short crack growth behaviour of the low Si alloy was observed by Moffat [1] to be significantly influenced by their porosity. This pore induced short crack behaviour was however not observed in the 6.9 wt.% Si alloy.

These studies therefore indicate that lowering Si levels reduces the role of Si particles in fatigue crack initiation. However, this is accompanied by increased porosity, which then dominates fatigue behaviour especially for the low Si alloy. Although the 6.9 wt.%Si alloy did not show pore induced short crack growth behaviour, Moffat [1] observed significant interactions between the crack and eutectic Si structures. It has been shown in a separate publication [8] that the Si particle size and shape distribution are significantly transformed after hipping the strontium modified version of this alloy. It is therefore expected that this Si particle transformation may translate to profound differences in the short crack growth micromechanisms. This paper presents results obtained from a short crack growth study of the hipped version of the Sr-modified 6.9 wt.%Si alloy. The results are then compared with previous work carried out by Moffat [1] on the unhipped alloy. The alloy investigated is denoted as Al7Si-Sr in Table 1. Results from an investigation on the hipped version of the 0.67 wt.% Si alloy (i.e. Al0.7Si alloy in Table 1) are reported elsewhere [9].

2. Experiments

2.1 Materials

The alloy investigated (Al-7Si-Sr in Table 1) was supplied as unfinished pistons in the hipped and unhipped conditions. The hipped pistons were supplied after being subjected to a hipping and heat treatment procedure that involved holding at 490°C and 100 MPa for 4 h, solution treatment at 480°C for 2 h, a water quench and finally ageing for 8 h at 230°C. The unhipped pistons were supplied after aging at 230°C for 8 h.

2.2 Short crack fatigue tests

Short crack fatigue tests were carried out using 12x12x80 mm plane bend bar specimens, which were sectioned from the central portion of each piston crown and aged at 260°C for 100 h prior to testing to simulate in-service thermal exposure. The top surface of each specimen was polished to ~0.05 µm finish to allow free initiation from microstructure features and facilitate accurate monitoring of the crack-microstructure interactions. The edges of the specimens were also rounded off by grinding and polishing to 0.25 µm to minimise chances of initiation from the edges. Room temperature tests were carried out in four point bend with a span of 15 mm on a servohydraulic Instron 8502 machine at a load ratio of 0.1

using a sinusoidal waveform of 15 Hz. The formation and growth of fatigue cracks was monitored by periodically interrupting the test and taking acetate replicas of the polished tensile top surface of the specimens.

The loading conditions were such that the maximum near-surface tensile stresses (σ_{\max}) were above the 0.2% proof stress of the material ($\sigma_{0.2}$ for the alloy is ~ 110 MPa). A small top surface layer was therefore plastically deformed, but the bulk of the specimen remained elastic. The maximum stress was approximated by comparing actual strain on the specimen surface (obtained using strain gauges) with the corresponding stress on the tensile stress-strain curve. Finite element (FE) calculations were also carried out in ABAQUS to confirm the through thickness stress and strain distribution. The FE calculations were based on monotonic uniaxial tensile stress-strain data for the material model (assuming isotropic hardening behaviour) applied to the appropriate bend bar geometry. The models were meshed using C3D20R elements ensuring that results were independent of mesh density.

In the current study, several cracks in two specimens were characterised in the hipped Al7Si-Sr alloy. Both specimens were tested under similar loading conditions of a maximum stress and strain of 148 MPa and 0.85, respectively. One specimen was loaded until it failed after 125141 cycles while the other one was stopped just before failure after 94000 cycles. Table 2 shows the testing parameters including the test carried out in a previous study by Moffat [1]. The observed crack initiation life (N_i) and total fatigue life (N_f) of the tested specimens are also indicated in the table.

2.3 Short crack data analysis

The growth of several fatigue cracks on each specimen was investigated by examining the acetate replicas under an optical microscope. Optical images of the cracks on the replicas were taken and crack length measurements carried out using ImageJ. The crack growth data was analysed using the secant method to obtain da/dN values at various ΔK values calculated using the solution recommended by Scott and Thorpe [10]. X-ray microtomography of a secondary crack on an S-N test specimen of this alloy indicated that a/c is ~ 1.05 . The shape of the crack was therefore approximated to be semi-circular when computing ΔK values. This is in agreement with Moffat's [1] observations for the unhipped alloy.

2.4 Crack growth micromechanisms

The micromechanisms of short fatigue crack growth were investigated by examining the interaction of short fatigue cracks with microstructural features in the interrupted specimen and secondary cracks in the failed specimens. The microstructural features targeted were intermetallics, Si particles and even porosity. This investigation was carried out using optical microscopy and SEM coupled with EDX for phase analysis.

3. Results and discussion

3.1 Crack growth data

Figure 1 shows the short crack growth data for the hipped and unhipped alloy together with the corresponding long crack growth data for comparison. The figure shows that the short crack growth rates are generally much higher than long crack growth rates at corresponding values of ΔK . Moreover, significantly high growth rates are observed even at ΔK values

below the corresponding ΔK_{th} for long cracks. Frequent crack growth retardation and arrest events are also observed as shown more clearly in Figure 2 for selected cracks. However, Figure 2a indicates that crack arrest events were not observed in the test interrupted after 94000 cycles although the loading conditions were similar to the one tested to failure. This may be attributed to the crack observation (replication) intervals chosen during testing. Acetate replication for the specimen tested to failure was taken mostly at 1000 cycle intervals after the first 50000 loading cycles while 5000 cycle intervals were used (mostly) for the interrupted test. Note that the crack growth retardation observed in the hipped alloy exhibit a certain degree of periodicity as shown in Figures 2a and 2b. This is discussed further in section 3.2.

Figures 1 and 2 also show that the short crack growth rates for the hipped alloy are generally lower compared with those for the unhipped alloy. However, the unhipped alloy had been tested at a higher maximum stress of $\sigma_{max}=170$ MPa (159% $\sigma_{0.2}$). This specimen failed after 45252 cycles as opposed to 125141 cycles for one of the hipped specimens. The slightly higher growth rates for the unhipped alloy is therefore be attributed to the higher applied stress. The stress effect on short crack growth has also been observed in the low Si piston alloy (Al0.7Si) [9]. Similar observations have also been reported in a 319 type alloy by Caton et al [11] and in A356 by Plumtree and Schaefer [12]. The loading conditions used in this work result in a plastically deformed layer near the surface of the specimen right from the first loading cycle. The magnitude of this surface layer deformation naturally depends on the applied stress. Previous reports [11,13,14] suggest that this stress dependent global and local crack tip plasticity can accelerate the growth of short cracks and is therefore be the cause of the stress dependent results observed in this alloy.

3.2 Crack growth micromechanisms

Fatigue cracks in this alloy were observed to initiate from intermetallic particles within the first 100 cycles in both specimens investigated as illustrated in Figure 3. This figure shows a fatigue crack forming from a debonded Al_9FeNi particle. A replica taken after 10 cycles indicated that debonding was already in progress although it clearly did not occur during the first cycle as shown in Figure 3a. The crack is ~ 60 μm by 1000 loading cycles and ~ 110 μm at 5000 cycles after which it is retarded (cf. the crack position at 10000 cycles). It can be seen that retardation occurs at both tips although the left tip seems to have already grown past the eutectic region after 5000 cycles as shown by the optical and SEM images in Figures 3b & 3c. It is possible that this tip may have encountered a grain boundary. However, a superimposed grain boundary map would be required to confirm this speculation. The retardation at the right tip can however be attributed to the resistance provided by the intermetallics and Si particles encountered by the crack at this point.

Figure 4 shows another set of cracks that initiated in the same specimen. The multiple cracks which are seen to occur in close proximity to each other in Figure 4a do indeed eventually coalesce at later stages of crack growth as shown in Figure 4b. Figures 4c and 4d show high magnification SEM images of these initiation sites in which it is clear that most of these cracks occurred via fracture of Al_9FeNi particles. However an $Al_2Ni(CuSiZrFeMg)$ particle can be seen at one of the initiation sites in Figure 4d. A replica taken at 110 cycles indicated that debonding of this particle had already occurred simultaneously with the adjacent Al_9FeNi particle. The cracks are clearly visible on the acetate replica shown in Figure 4a after 1000 cycles.

Figure 5 shows that there is significant damage at the eutectic Al-Si regions where cracks (or slip bands) can be seen emanating from Si and intermetallic particles. However, most of the Si particles preferentially debond rather than fracture as shown in Figures 5b and 5c. This is true even at crack locations fairly remote from the initiation site as shown in Figure 5b. It is therefore not surprising to observe that the crack preferentially propagates through the Al/Si interface when it encounters Si particles within the eutectic region or along the periphery of the Al-Si eutectic region.

Figure 6a shows the full profile of cracks A and B shown in Figure 4a after the test was stopped (at 94000 cycles). Both cracks are seen to have fully coalesced by this time with significant damage being observed at the coalescence region. Replica records indicated that the monotonic plastic zones of these cracks overlapped after only 20000 cycles and actual crack tip overlap occurred after 45000 cycles although uncracked ligaments are still observed even after 94000 cycles as shown in Figure 6a and more clearly in Figure 4b. Crack coalescence provides significant challenge in ΔK calculations due to the presence of these uncracked ligaments as well as the uncertainty on the actual crack shape. However, ΔK was estimated based on previous reports [15] that recommend treating the two cracks as fully coalesced as soon as their monotonic plastic zones overlap. A comparison of the different cracks in the two specimens tested for this alloy indicated that the growth rates of coalescing and non-coalescing cracks fell within the same scatter band.

The growth rates of the individual outer tips (A_{tip1} & B_{tip2}) of the coalesced crack were calculated and presented against the corresponding loading cycles and ΔK as shown in Figures 6b and 6c. The growth rate retardation points along the crack profile were then identified by comparing Figure 6a with Figures 6b and 6c. It is evident from this comparison that crack growth retardation was mainly associated with crack-microstructure interaction at the Al-Si eutectic regions. This observation is confirmed in Figures 7 and 8 which present a similar analysis for two other cracks of this alloy selected from each of the two specimens tested. One of the few exceptions is the crack growth retardation seen to have occurred after ~85000 cycles. This occurred at the large unusual crack deflection within the α -Al matrix shown in Figure 5a. The figure shows that the deflection may not be entirely attributed microstructural features. However, the retardation could in itself be associated with the deflection since its magnitude may be enough to cause a drop in the effective ΔK (mode I) at the crack tip. Similar deflections, but of smaller magnitude, are also observed at crack retardation events after 20000 and 50000 cycles. However, these are clearly associated with crack interaction with eutectic regions.

The large crack deflection at 85000 cycles could be partly explained in terms of slip band cracking as illustrated in Figure 5a. A section of the crack within the deflection seems to be along a slip band at ~45° to the tensile loading direction. Similar slip band associated cracking and deflections can be seen at other locations along the crack. Moreover, there is clearly an intermetallic particle adjacent to the crack on the left side which may have facilitated that section of the deflection via a possible decohesion mechanism beneath the surface. This seemingly unusual deflection may therefore be due to a combined influence of slip band cracking and crack-microstructure interaction. Similar slip band associated crack growth and deflection are illustrated in Figure 8a. In the web version of this paper, a replica video animation of this crack is provided as Figure A1. The animation shows a chronological development of the crack and provides a clear picture on the genesis of the various deflections along the crack, which is otherwise difficult to discern by just looking at the final crack profile. The replica animation shows that there are several cases of microcracking

ahead of the main crack which eventually lead to intermittent coalescence events that define some of the deflections and the final crack profile. The microcracks originate mainly from cracked intermetallics and propagate along slip bands emanating from these particles at $\sim 45^\circ$ to nominal crack plane.

Evidence of slip bands emanating from intermetallic particles has previously been reported for a typical Al-Si piston alloy. In particular, slip lines were observed emanating from the tips of cracks at particles and oriented at $\sim 45^\circ$ to the loading direction [8]. Moreover, the early growth of short cracks into the Al matrix was seen to be controlled by these slip lines [8]. Previous work on other commercial Al alloys has also shown that fatigue cracks that initiate from inclusions or 2nd phases often seem to be associated with localised slip bands that impinge on the particles [16]. A good example of this can be found in Kung and Fine [17] where fatigue cracks were observed to initiate along slip bands emanating from inclusions in a 2024-T4 aluminium alloy. This type of slip banding has indeed been predicted to occur adjacent to pores or failed particles via finite element analysis [18,19]. It is therefore expected that cracked particles ahead of the main crack front will significantly influence its growth behaviour.

The evidence provided so far indicates that short cracks in this alloy preferentially propagate along the Al/particle interfaces whenever they encounter such particles. However, cases of propagation through cracked particles are still observed although some of these are clearly associated with prior secondary crack initiation as shown by the replica animation in Figure A1 (available in the web version). This result is consistent with observations of precipitate free zones around particles observed in these alloys [8]. Similar precipitate free zones around intermetallics have previously been observed in a typical piston alloy [20]. The presence of this zone implies that the Al matrix around the particles is softer than that in the bulk. Interface failure is therefore expected to occur preferentially because of the combined effect of a softer matrix and higher local stresses due to load transfer effects of the intermetallics. However particle fracture does occur in cases where the particle size and orientation are favourable for efficient load transfer as discussed elsewhere [21]. It is indeed severally reported [22] that larger and elongated particles tend to fail more easily and those oriented such that their major axis is parallel to the loading direction preferentially failure via fracture as opposed to debonding [23].

The crack retardations observed at particles are therefore partly associated with forced deflections as the crack seeks to propagate through the weak interfaces and as such will depend on the particle size and orientation relative to the plane of the crack tip. Uncracked particles oriented normal to the crack plane are expected to be effective barriers and the crack will be forced to deflect sharply in order to bypass the particle or continue to be arrested until the particle eventually fails. On the other hand, particles ahead of the crack tip which are oriented parallel to the crack plane are expected to offer least resistance along their interface. Moreover, previously failed particles (debonded or fractured) seated ahead of the crack tip will naturally provide the weakest path.

Contrary to Moffat's observations on the unhipped alloy [1], significant damage was observed around eutectic Si particles in the hipped alloy and crack propagation within the eutectic region was preferentially through the Al/Si interface. This is consistent with various previous reports on Al-Si alloys [12,23,24]. The eutectic region in this alloy contains a cluster of both Si and intermetallic particles. Measurements show that the volume fraction of hard particles in this region ($\sim 35.1\%$) is $\sim 80\%$ higher than the average ($\sim 19.4\%$) [25]. Moreover,

the interparticle spacing within this region ($\sim 2.9 \mu\text{m}$) is significantly smaller than the average ($\sim 18 \mu\text{m}$). These particle clustered regions are therefore in a highly constrained state in which the matrix material trapped between the particles is shielded from plastic deformation [26]. This leads to an overall load shedding effect from particle poor to particle rich regions [27] thus increasing the local stresses in these stiffer regions. This in turn increases the propensity for damage to occur as indeed observed in the eutectic regions of this alloy.

Moreover, the modified Si particle network after hipping, is expected to significantly affect how load is transferred to the particles [21]. As previously reported [8,25], hipping transforms the Si particles from a fibrous coral-like interconnected network to more rounded and discrete particles. These particles are more likely to debond than fracture considering their relatively small size and rounded morphology [21]. It is therefore expected that crack growth would preferentially seek out these debonded regions within the eutectic since they provide a weaker path. However, eutectic regions as a whole may behave as effective crack growth barriers as observed in the hipped alloy investigated. The effectiveness (as a barrier) of any given eutectic region encountered by a crack tip depends on the extent of particle clustering (Si and intermetallics) as well as whether there are favourably oriented damage sites. These damaged or cracked regions within the eutectic can provide a weak path along which the main crack tip can channel through as proposed by Moffat [1]. The presence of such crack channelling would render the eutectic region impotent as pertains to crack growth retardation. This may explain why crack retardation was not always observed at the eutectic regions in this study. However, confirmation of this requires grain boundary mapping along the crack profile of the hipped Al7Si-Sr alloy to ascertain the possible role of grain boundaries on crack retardations as reported elsewhere for the hipped low Si Al0.7Si alloy [9].

4. Conclusions

The short crack behaviour of a hipped Al7Si-Sr model piston alloy was investigated and compared with previous results on its unhipped counterpart. Short crack growth exhibited classical behaviour with significant scatter and frequent crack decelerations/arrest events. The cracks were also observed to grow at faster rates than long cracks at equivalent ΔK values and also grew at significantly higher rates even when ΔK was far below the ΔK_{th} for long cracks.

Frequent crack growth retardations were observed at intermetallics particles and eutectic Al-Si regions. The cracks were observed to preferentially grow along Al/particle interface whenever they encountered such particles. This observation remained true for both intermetallic particles and eutectic Si.

Acknowledgement

The first author acknowledges the Faculty of Engineering and the Environment of the University of Southampton and the University of Nairobi for their financial support when this work was carried out. Dr Katherine Soady is also thanked for her assistance with the FE modeling to establish the local stress states. Finally, the authors would like to thank Professor Ian Sinclair for fruitful discussions that helped to improve the quality of this work.

References

- [1] Moffat, A.J., Micromechanistic analysis of fatigue in aluminium silicon casting alloys, PhD Thesis, School of Engineering Sciences, 2007, University of Southampton.
- [2] Reichstein S, Konrad P, Kenningley S, Dornenburg FTH. *ATZautotechnology* 2008; 8;42.
- [3] Moffat AJ, Mellor BG, Chen CL, Thomson RC, Reed PAS. *Mater Sci Forum* 2006;519-521;1083.
- [4] Chen CL. Characterisation of intermetallic phases in multicomponent Al-Si alloys for piston applications, PhD Thesis, IPTME, Loughborough University, 2006.
- [5] Moffat AJ, Barnes S, Mellor BG, Reed PAS. *Int J Fatigue* 2005;27;1564.
- [6] Joyce MR, Styles CM, Reed PAS. *Int J Fatigue* 2003;25;863.
- [7] Moffat A J, Mellor BG, Sinclair I, Reed PAS. Short crack and near threshold fatigue behaviour of Al-Si casting alloys. 12th International Conference on Fracture, 12-17 July 2009, Ottawa, Ontario, Canada. Vol. 4, p.3081-3090.
- [8] Mbuya TO, Sinclair I, Moffat AJ, Reed PAS. *Mater Sci Eng A* 2011;528;7331.
- [9] Mbuya TO, Gu KY, Thomson RC, Reed PAS. Interaction of short fatigue cracks with intermetallic particles and grain boundaries in a cast Al piston alloy. Submitted to *Int J Fatigue*
- [10] Scott PM, Thorpe TW. *Fatigue Fract Eng Mater Struct* 1981;4;291.
- [11] Caton MJ, Wayne Jones J, Boileau, JM, Allison JE. *Metall Mater Trans A* 1999;30;3055.
- [12] Plumtree A, Schafer S. Initiation and short crack behaviour in aluminium alloy castings, In: *The Behaviour of Short Fatigue Cracks*, J.K. Miller and E.R. De los Rios, Editors. 1986, Mechanical Engineering Publications, p. 215-227.
- [13] Hudak SJ, Chan KS. In Search of a driving force to characterize the kinetics of small crack growth, In: *Small Fatigue Cracks*, R.O. Ritchie and J. Lankford, Eds, 1986, The Metallurgical Society, Santa Barbara, California. p. 379-403.
- [14] Edwards L, Zhang YH. *Acta Metall et Mater* 1994;42;1413.
- [15] Lefebvre F. Micromechanical assessment of fatigue in airframe fusion welds, PhD Thesis, School of Engineering Sciences, 2003, University of Southampton.
- [16] Kung CY, Fine ME. *Metall Mater Trans A* 1979;10;603.
- [17] Fine ME, Ritchie RO. Fatigue-crack initiation and near-threshold crack growth. in *Fatigue and microstructure*, 1978 ASM Materials Science Seminar. 1978. St. Louis, Missouri: ASM.
- [18] Fan J, McDowell DL, Horstemeyer MF, Gall K. *Eng Fract Mech*;2003;**70**;1281.
- [19] Gall K, Horstemeyer MF, Degner BW, McDowell DL, Fan J. *Int J Fract* 2001;108;207.
- [20] Bischofberger U, Neite G, Exner HE. *Key Eng Mater* 1991;44;333.
- [21] Starink MJ. *Mater Sci Eng A* 2005;390;260.
- [22] Verdu C, Cercueil H, Communal S, Sainfort P, Fougères R. *Mater Sci Forum* 1996;217-222;1449.
- [23] Gall K, Yang N, Horstemeyer M, McDowell DL, Fan J. *Metall Mater Trans A* 1999;30;3079.
- [24] Shiozawa K, Tohda Y, Sun SM. *Fatigue Fract Eng Mater Struct* 1997;20;237.
- [25] Mbuya TO. Analysis of microstructure and fatigue micromechanisms in cast aluminium piston alloys. PhD Thesis, Faculty of Engineering and the Environment, 2011, University of Southampton.
- [26] Wilkinson DS, Maire E, Embury JD. *Mater Sci Eng A* 1997;233;145.
- [27] Wilkinson DS, Maire E, Fougères R. *Mater Sci Eng A* 1999 ;262;264.

Tables

Table 1 Compositions (in wt. %) of the model cast aluminium piston alloys.

Alloy	Si	Cu	Ni	Mg	Fe	Mn	Ti	Zr	V	P	Sr
Al12.5Si	12.45	3.93	2.78	0.67	0.44	0.03	0.01	0.05	0.04	0.005	0
Al7Si-Sr	6.9	3.89	3.0	0.62	0.22	0.03	0.01	0.05	0.05	0.005	0.015
Al0.7Si	0.67	3.91	2.99	0.80	0.21	0.05	0.01	0.01	0.01	0.005	0

This alloy was supplied in unmodified and Sr-modified conditions. The alloy investigated in this work is the Sr-modified version.

Table 2 Short fatigue crack growth loading conditions and cycles to failure.

Alloy (& Specimen No.)	σ_{\max} (MPa)	$\sim N_i$	N_f	$\sim N_i/N_f$ (%)
HIPAl7Si-Sr (1)	148	<100	94000 (stopped)	<1%
HIPAl7Si-Sr (2)	148	<100	124523	<1%
Al7Si-Sr (ref. [1])	170	<5000	45252	11.0

Figures

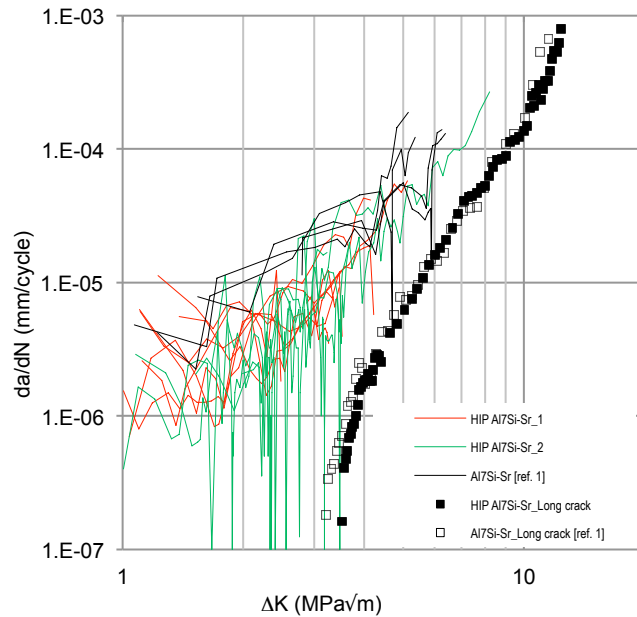


Figure 1 Short crack growth data for all the cracks analysed in the hipped alloy compared with the unhipped material and the corresponding long crack growth data.

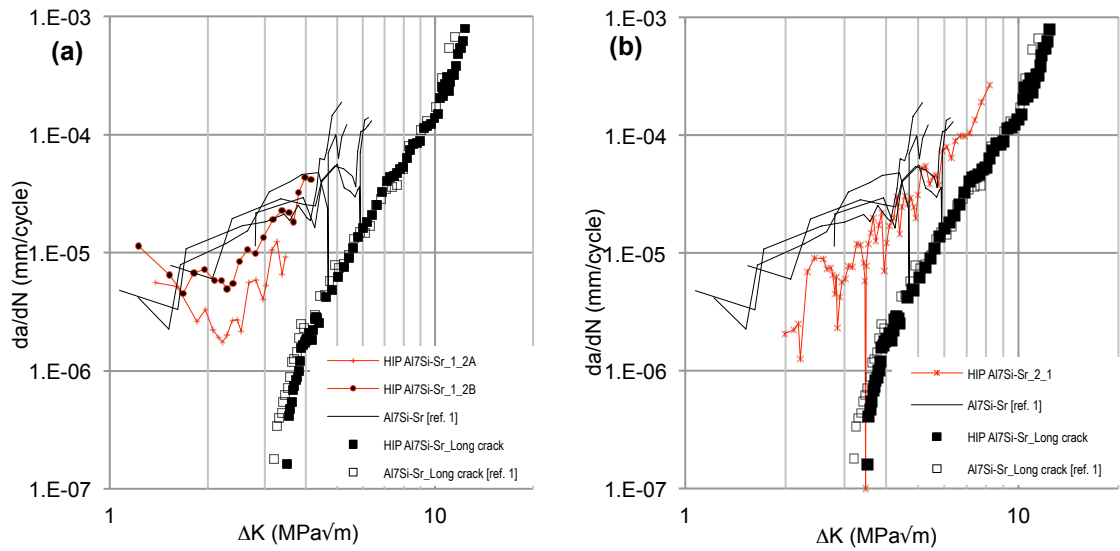


Figure 2 (a) Short crack growth data for the hipped alloy showing periodicity in crack growth retardations in (a) the specimen interrupted at 94000 cycles and (b) the specimen tested to failure at 125141 cycles.

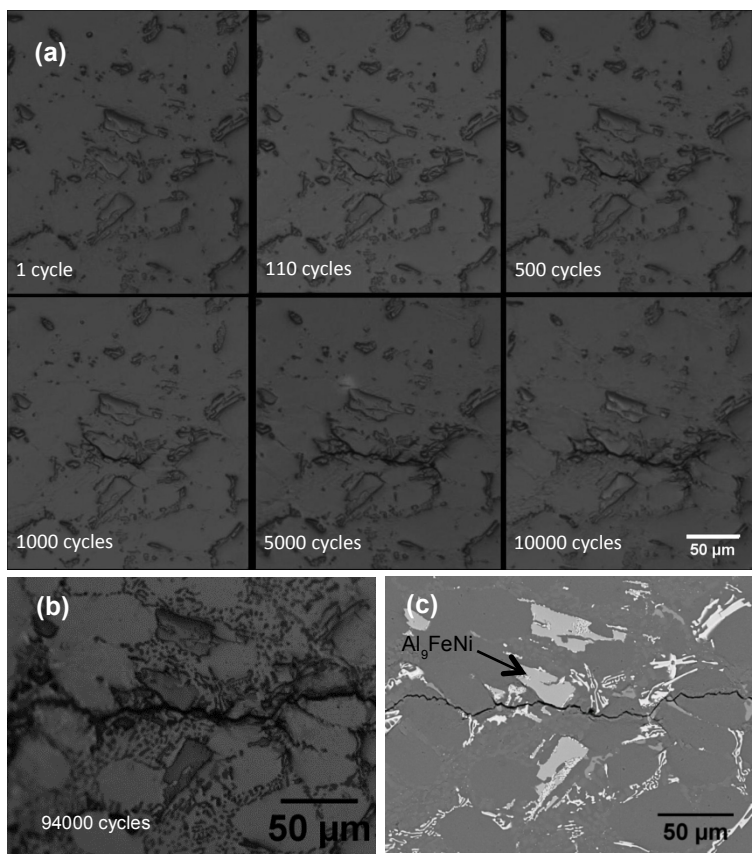


Figure 3 (a) A replica record of the initiation and early growth of a short crack in a hipped specimen that was stopped after 94000 cycles. Optical and SEM images of the region around the initiation site are shown in (b) and (c) respectively. Initiation occurred via decohesion of an Al_9FeNi particle. Note that the replica does not clearly show the eutectic Si network as seen in the optical image and to some extent in the SEM image.

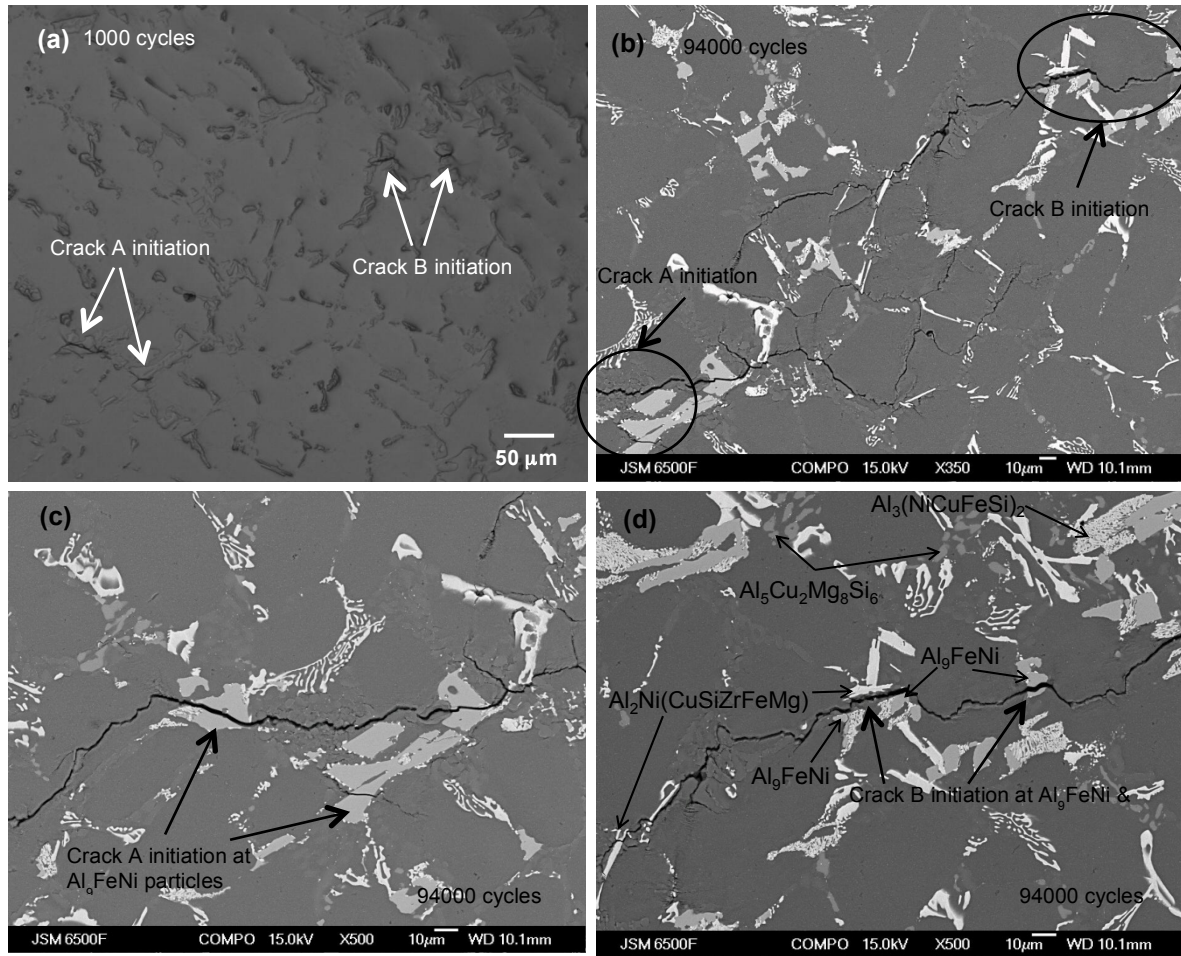


Figure 4 (a) A replica showing initiation and early growth of other short cracks in the specimen that was loaded up to 94000 cycles. These two cracks eventually coalesced as shown in the SEM image in (b). (c) and (d) show higher magnification SEM images of the two initiation sites in which several phases are identified. Crack A initiated by fracture of Al_9FeNi while initiation of crack B was via debonding and fracture of two Al_9FeNi particles and an $\text{Al}_2\text{Ni}(\text{CuSiZrFeMg})$ particle.

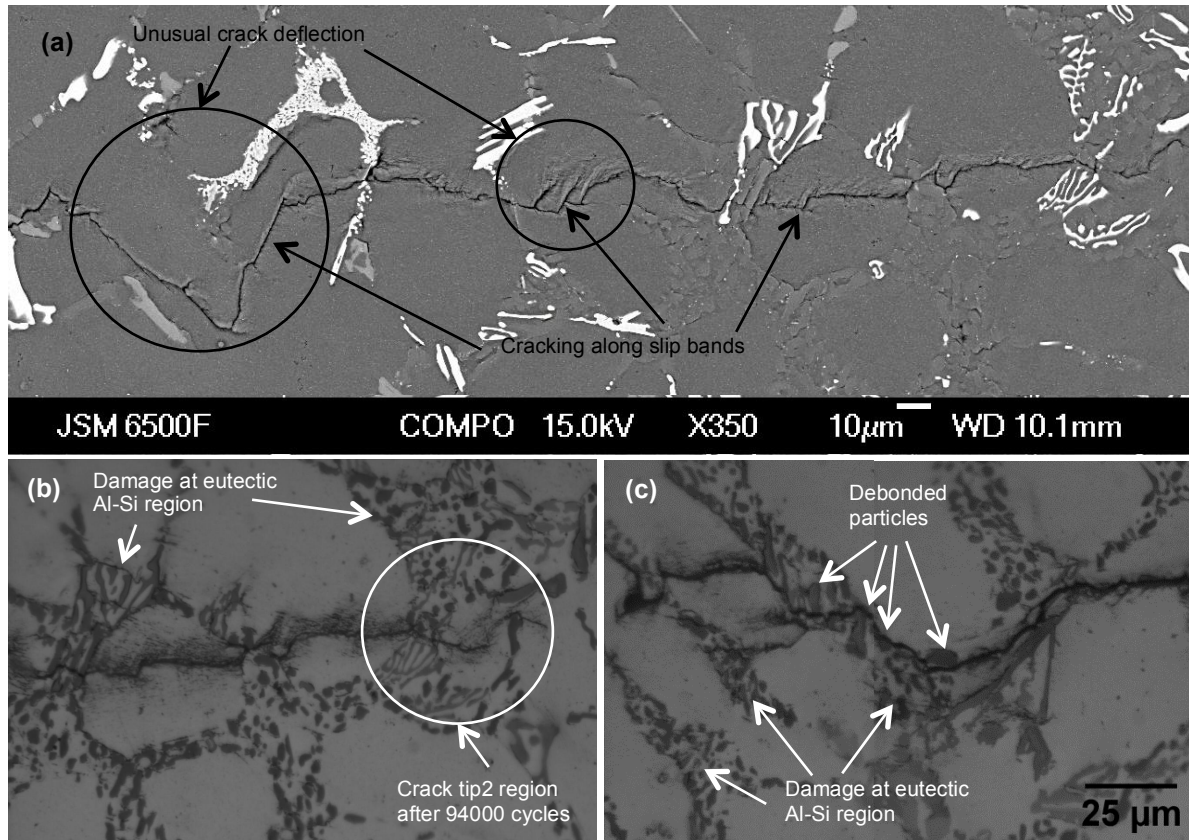


Figure 5 (a) SEM and optical images of the near tip region of crack B showing crack deflections and cracking along slip bands. (b & d) Optical images of the near tip region of crack B and a section of crack A indicating that growth through the eutectic Al-Si regions is mainly via Si particle debonding. Note the damage at eutectic regions.

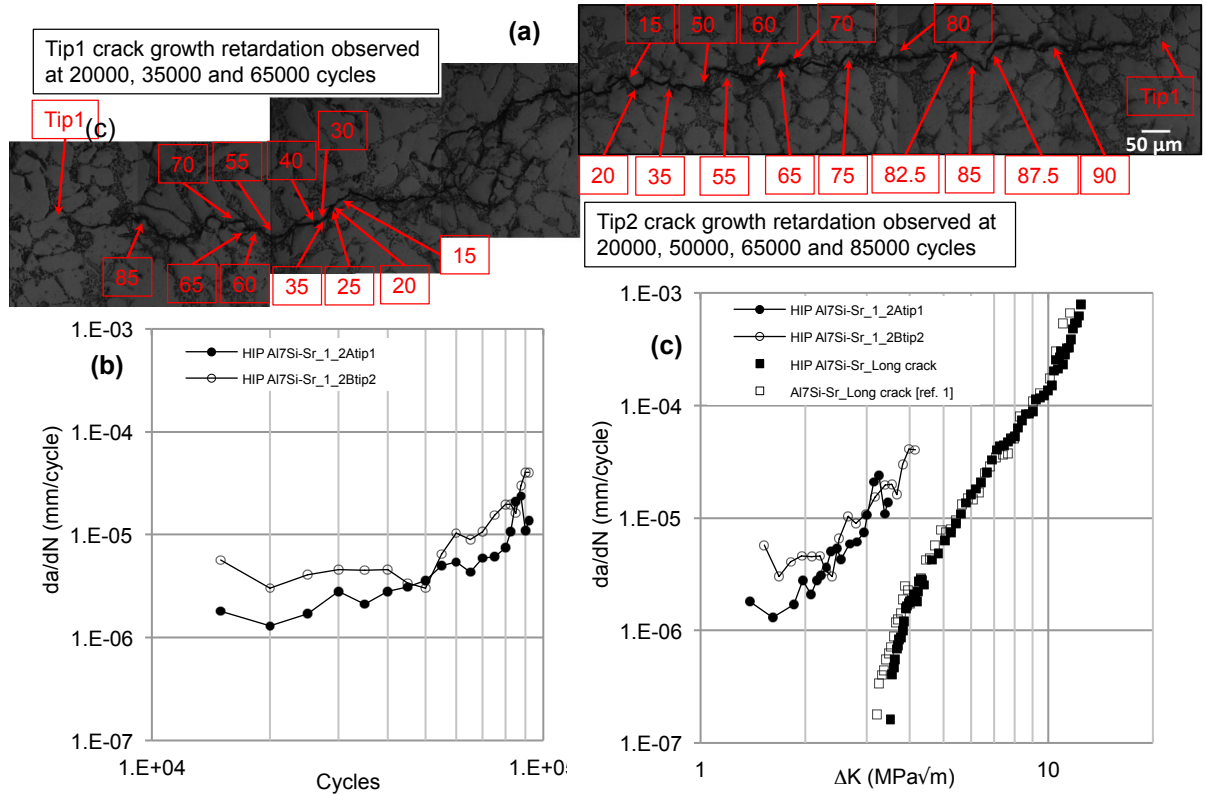


Figure 6 (a) Crack-microstructure interaction of the outer tips (Atip1 & Btip2) of the short cracks in Figure 4a. (b) & (c) Short crack retardation and arrest events of both tips vs. the corresponding loading cycles (in units of 1000 cycles) and ΔK .

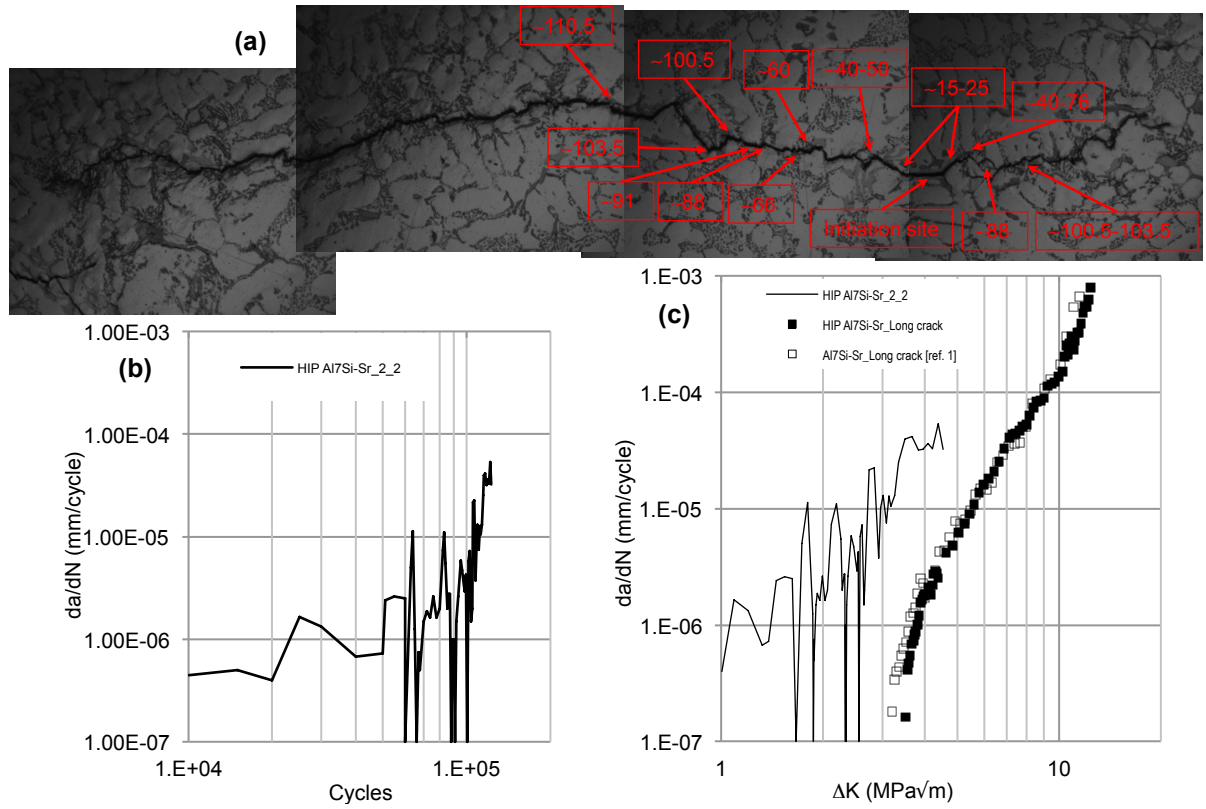


Figure 7 (a) Crack-microstructure interaction of another short crack for the HIPped alloy. (b) & (c) indicate short crack retardation and arrest events of the crack in (a) vs. the corresponding loading cycles (in units of 1000 cycles) and ΔK .

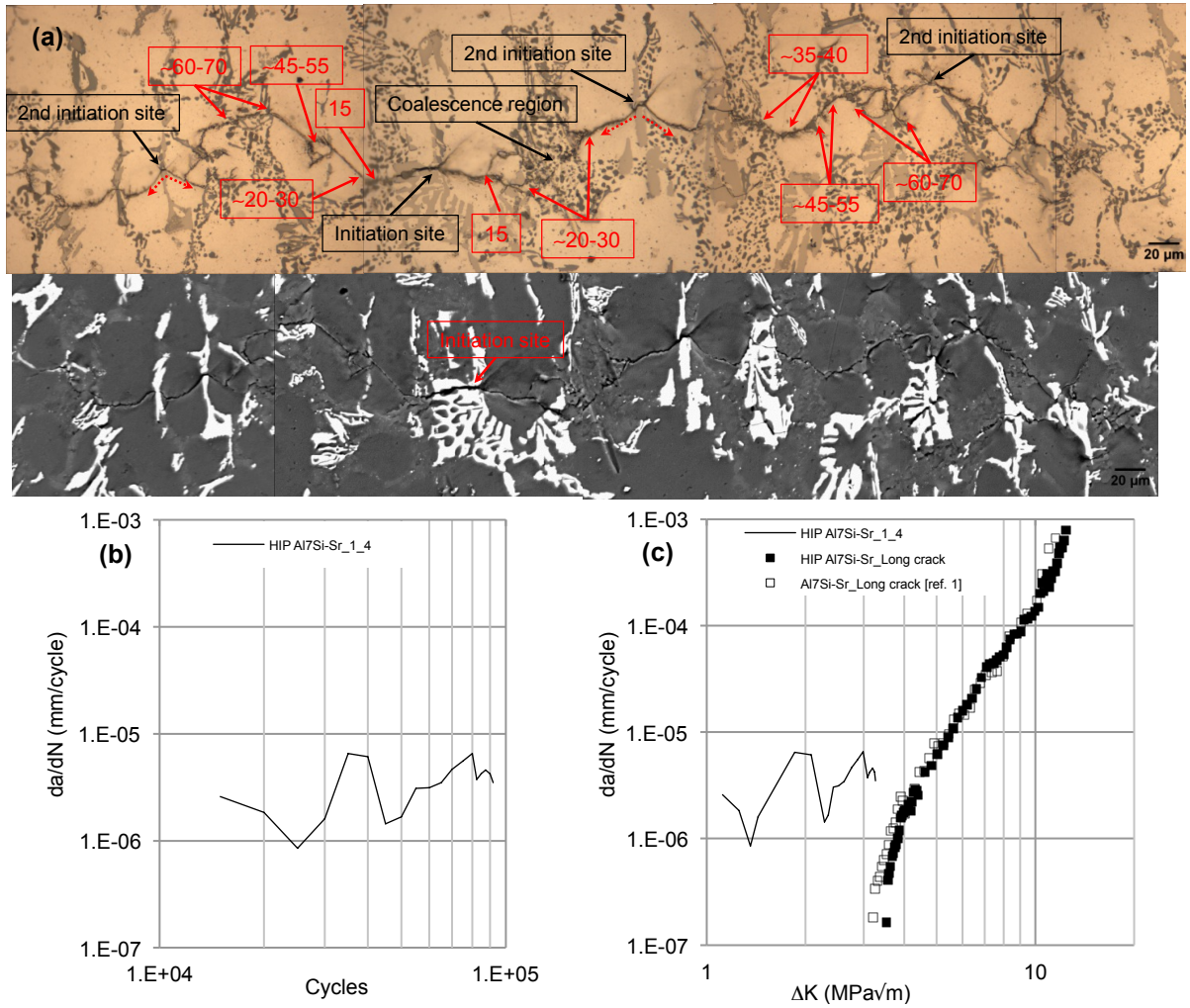


Figure 8 (a) Crack-microstructure interaction of another short crack for the hipped alloy. (b) & (c) Indicate short crack retardation and arrest events of the crack in (a) vs. the corresponding loading cycles (in units of 1000 cycles) and ΔK . A replica video animation of this crack showing its chronological development is provided in Fig A1 as supplementary material in the web version of the paper.

Figure A1 (Provided as a separate video clip) A replica video animation of the crack presented in Figure 8. The animation shows the interaction of this crack with microstructure during its chronological development.